Journal of Alloys and Compounds 604 (2014) 175–180

Contents lists available at ScienceDirect

Journal of Alloys and Compounds

journal homepage: www.elsevier.com/locate/jalcom

Review

Uniaxially aligned ceramic nanofibers obtained by chemical mechanical processing

R. Tararam [a], C.R. Foschini [b], F.B. Destro [c], A.Z. Simões [c,*], E. Longo [a], J.A. Varela [a]

[a] Univ Estadual Paulista – UNESP – Instituto de Química, Rua Prof. Francisco Degni n° 55, CEP 14800-900 Araraquara, SP, Brazil
[b] Univ Estadual Paulista – UNESP – Faculdade de Engenharia de Bauru, Dept. de Eng. Mecanica, Av. Eng. Luiz Edmundo C. Coube 14-01, CEP 17033-360 Bauru, SP, Brazil
[c] Univ Estadual Paulista – UNESP – Faculdade de Engenharia de Guaratinguetá, Guaratinguetá 12516-410, SP, Brazil

ARTICLE INFO

Article history:
Received 19 November 2013
Received in revised form 21 March 2014
Accepted 24 March 2014
Available online 2 April 2014

Keywords:
ZnO
CuO
Nanofiber
Inorganic/polymer composites

ABSTRACT

For this study, we investigated a simple method to generate well aligned nanofibers over large areas using an organic polymer stretched over the substrate surface With this method, ZnO and CuO 3D parallel nanowire arrays were successfully prepared by calcinations of the polymer fibers. X-ray diffraction (XRD) analysis revealed that the copper oxide has a monoclinic structure while the zinc oxide has a hexagonal structure. Scanning electron microscopy (SEM) analysis showed ceramic nanofibers with an average diameter of 120 nm which were composed of small nanoparticles which are 10 nm in diameter. The ability to obtain uniaxially aligned nanofibers reveals a range of interesting properties with potential applications for sensors, catalysts and energy technologies.

Contents

1. Introduction

Several advantages of using nanofibers and nanowires are reported in the literature. Due to their high aspect ratio, the control of surface chemical interactions is critical for sensors and catalysts. Although few authors have successfully obtained the deposition of oriented fibers, randomly distributed nanofibers can easily be obtained by electrospinning; e.g., ZnO [1–3] and CuO [4–6] Dabirian et al. [7] employed centrifugal forces during electrospinning to align fibers while Li et al. [8] reported the application of electric fields in electrodes during the deposition by electrospinning to achieve fiber orientation. In both cases, problems with low deposition rates in small surface areas created difficulties for practical applications. Today, gas sensors are available in the market for automotive and health applications as well as more traditional areas such as alarms sensitive to toxic or explosive gases. To develop better, cheaper, faster, more sensitive and selective sensors, new research is focused on nanostructured sensors [9,10]. There is a demand for new functional materials, different ways of preparation and contact configurations. Researchers are investigating new active gas sensors with appropriate characteristics for their specific functionalities [11–15].

With recent progress in the nanoscience field, micro- and nanosensors of metallic oxide are produced; e.g., the production and manipulation of metallic oxide nanowires. However, manipulating

* Corresponding author.
E-mail address: alezipo@yahoo.com (A.Z. Simões).

http://dx.doi.org/10.1016/j.jallcom.2014.03.149
0925-8388/

individual nanowires to apply them to large-scale production poses a huge problem. Due to their small dimensions, micro- and nano-sensors can be heated locally which facilitates energy savings as well as better integration of different materials, when larger selectivity is desired [16,17].

These quasi-one-dimensional Q1D structures have a high aspect ratio (surface area per volume) and demonstrate a superior sensitivity to chemical surface processes. In addition, Q1D structures not only have characteristics of the macroscopic crystal such as piezoelectricity, chemical sensibility and photodetection, but also introduce new properties associated with the confinement of their dimensions and their high geometric anisotropy [18,19]. Several previous studies illustrate that nanowires show potential applications as gas sensors, chemical and biological sensors, micro lasers and displays. Nanowires based on super-lattices and p–n junctions in a single nanowire have previously been researched. The development of nano-field effect transistors (FETs), light emitting diodes (LEDs), bipolar junction transistors and logical circuits is quite promising with potential applications for metallic oxide nanowires in the nano-device area [20].

Charifi et al. [21] employed ab initio techniques to investigate structural, electronic and optical properties of ZnO compounds; they reported that 3d orbitals of the Zn atom were treated as the valence band (VB) with an indirect band gap of 1.47 eV. Bouderbala et al. [22] synthesized undoped ZnO thin films of different thicknesses by radio frequency (r.f.) sputtering to study the effect of thickness on their structural, morphological, electrical and optical properties. These authors noted an increase in the grain size versus the thickness while electrical properties measurements revealed behavior which is very dependent upon thickness. Optical measurements confirmed that all samples have a strong transmission which is higher than 80% in the visible range. A slight shift in the absorption edge towards large wavelengths was observed as the thickness increased; this result confirms that the band gap decreases slightly from 3.37 to 3.32 eV, and the film thickness varies from 0.32 to 0.88 mm. In other research, Reshak et al. [23] obtained inorganic ZnO nano-crystallite (NC) which was incorporated into photopolymer matrices (7.5% by weight) and optically treated by coherent bicolor nano-second laser pulses with Er^{3+} glass laser lines at 1.54 and 0.77 μm. Sufficiently good effective second-order susceptibility coefficients (up to 2.8 pm/V) at wavelengths of 1.54 μm were achieved. The maximum second-order optical susceptibility was achieved for NC sizes equal to about 30 nm. Ozga et al. [24] studied photoinduced second harmonic generation (SHG) in Au nanoparticle-deposited ZnO (NC) films which they explored by applying a bicolor coherent treatment of a Nd-YAG laser with a wavelength of 1.06 μm and its SHG. These authors have established that the co-existence of ZnO and Au nanoparticles produces a substantially larger SHG output with respect to pure ZnO NC deposited on the glass substrate which reaches a second order susceptibility of about 23 pm V^{-1}. Better nonlinear optical susceptibilities were obtained during photo treatment at temperatures near 30–35 °C for Au doped samples; Samples without gold NCs are temperature-independent, and generally, an increasing in the temperature produces a decrease in the optical SHG. CuO nanowires were prepared on copper foil by thermal oxidation in air. The effect of annealing temperature and growth time on the nanowire morphology was investigated which revealed that the annealing temperature and the growth time are important in the CuO nanowire morphology such as the density, *t* length and diameter. The length and density of nanowires increase with prolonging growth time [25]. Du et al. [26] prepared porous ZnO photocatalysts by a facile method; i.e., the thermal treatment of zeolitic imidazolate framework-8. The calcination temperature and time significantly influenced the ZnO morphology, composition and pore structure. Photocatalytic activities of as-prepared ZnO powders were evaluated in the degradation of methylene blue (MB) under a UV light in comparison with commercial anatase TiO_2 and Degussa P25 TiO_2. The surface area and crystallinity of porous ZnO obviously affected the photocatalytic activity of ZnO. The ZnO prepared at 500 °C for 5 h (ZnO-500-5) exhibited the highest photocatalytic activity which was higher than the photocatalytic activity of the commercial anatase TiO_2 and lower than the photocatalytic activity of Degussa P25 TiO_2.

ZnO nanofibers doped with different Al concentrations were fabricated by the electrospinning method; these nanofibers have a hexagonal structure with a diameter of about 150 nm. The nanofiber grain size decreases after La doping. PL spectra of all samples have two luminescence bands at green and orange centers. These bands can be attributed to oxygen vacancies and an excess of oxygen [27]. Zhao et al. [28] reported the fabrication of Mg doping on the crystal structure, morphology and optical properties of ZnO nanofibers obtained by the electrospinning method whereas the surface area-to-volume ratio is one or two orders of magnitude more than the ratio of continuous thin films. For this study, we investigated a simple and versatile method to develop ceramic nanofibers based on ZnO and CuO uniaxially aligned over large areas. One-dimensional structures were obtained as a result of both mechanical processing and the thermal treatment of organic fibers containing metallic precursors.

2. Experimental procedures

The novel approach to the spinning process described in this work differs from the well known electrospinning technique which was already studied earlier [29–31]. The typical electrospinning method consists of extruding a polymeric fluid from a needle in an electric field which was successfully exploited to generate thin fibers from a broad range of polymers. However, electrospun fibers are often collected as randomly oriented structures with slow deposition rates on small surface areas. This study establishes a new method which involves a combination of chemical and mechanical forces to a spinning process over larger surface areas and higher deposition rates. A special polymer which can be highly stretched between two moving plates to form filaments in the air gap was employed. An alternative configuration using two rolls spinning in contact facilitates continuous production of polymer ultrathin fibers which is related to a method for simultaneously spin stretching the polymer in the spinning device.

Fig. 1 displays the process flowchart of technical operations and illustrates the apparatus employed for fiber production. The initial step involves the preparation of the composite fluid which is formed from the polymer solution mixed with a metal salt solution (e.g., Cu^{2+} and Zn^{2+} ions). Then a drop of the composite fluid is dispersed on the roll surface (coating roll) to evaporate the solvent. This viscous polymeric coating can be stretched out mechanically by using the device shown in Fig. 1b which is composed of two cylinders rotating in contact (in opposite directions). Multifilaments of the fibers are formed in the air gap between the junction point of the cylinders and the substrate. A close inspection reveals that the fibers are always parallel and well aligned due to the extensional flow in the moving surface of the cylinders. The fibers are collected by correct positioning of the substrate, but there is still the possibility of using jets of compressed air to expel the fibers to obtain a random distribution which is similar to the electrospinning technique but with much larger deposition rates. The last step is the calcination of composite fibers above 500 °C to eliminate the organic material; only the desired metallic oxide remains in the form of wires. The process can also be used with more than one metallic cation in the stoichiometric composition so complex ceramic nanofibers can be obtained which results in promising perspectives (e.g., gas sensors: $CaCu_3Ti_4O_{12}$ [32], $NiFe_2O_4$ [33], $SrTiO_3$ [34]).

The complete process of fiber production (the spin-stretching technique) is limited by viscoelastic properties of the composite fluid. The stretchability of the composite can be altered depending of the metal solution added and the solvent used; i.e., stretching of at least 1 m without breaking the filament. Therefore, larger rolls could cover an area of 1 m^2 with fibers uniaxially aligned, and currently no technique exists whereby ceramic nanowires with these dimensions can be achieved,

Samples were characterized by field-emission scanning electron microscopy (FEG-SEM) (JEOL, Model 7500F) and energy dispersive spectroscopy (EDS) microanalysis. The phase characterization of these ceramic nanofibers was evaluated by XRD using Cu Kα radiation (diffractometer Model RIGAKU DMAX/2500 PC with a rotary anode operating at 150 mA and 40 kV). The crystallite size (d) of the metal oxide was calculated using Scherrer equation $d = k\lambda/\beta \cos\theta$, where k is constant, λ is wavelength of X-rays and β is the full width at half maximum (FWHM) reflections measured from slow scan, where θ is the diffraction angle of the main peak. TG

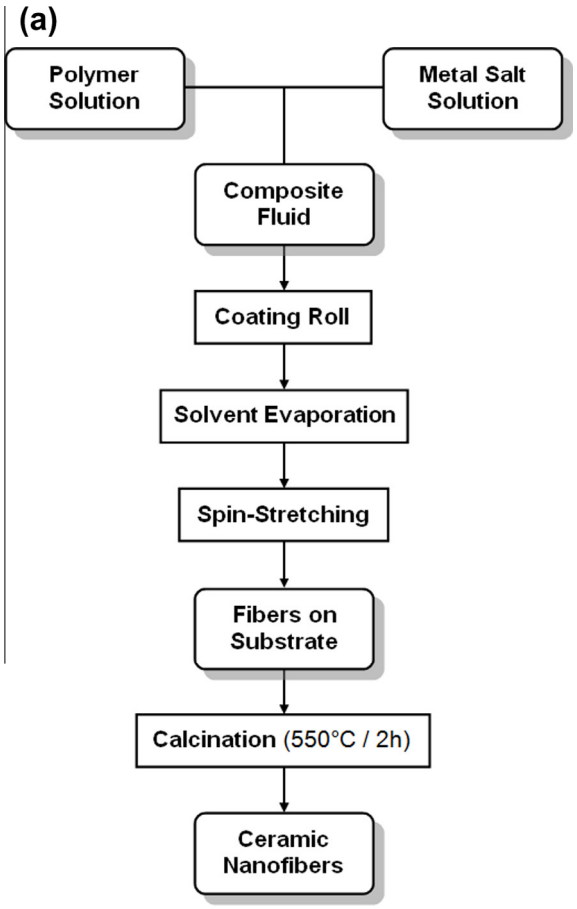

Fig. 1. (a) Process flowchart for the production of ceramic nanofibers; (b) schematic illustration of the apparatus used for the spin-stretching technique: (1) and (2) are rolls spinning in contact for polymer stretching, and (3) depicts multifilaments of fibers formed in the air gap.

analysis of the dry polymer was carried out with a Netzsch-409 STA apparatus with a heating rate of 10 °C/min under air atmosphere (flow rate 40 ml/min). FT-IR spectrum was recorded with a Bruker Equinox-55 instrument to obtain chemical information about dry polymer using KBr pellet method.

3. Results and discussion

3.1. Thermal analysis

Thermogravimetric analysis (TGA) of the polymer is shown in Fig. 2; the TGA results show that the dry polymer undergoes thermal degradation beginning at 540 °C with a total mass loss of 99.0%. Continuous mass loss is observed up to the decomposition

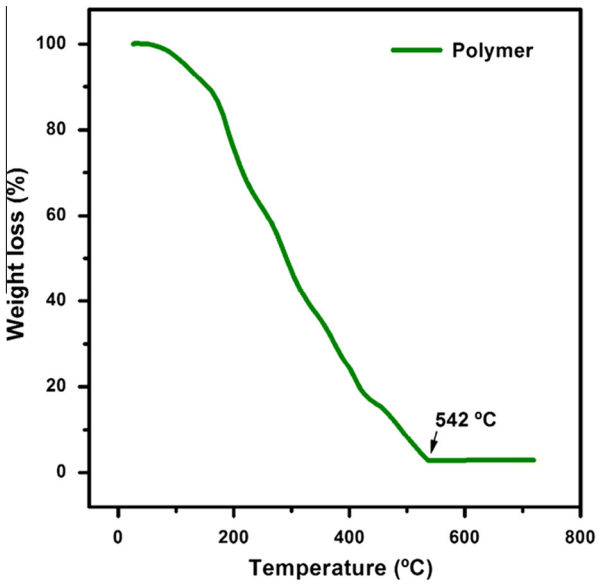

Fig. 2. TGA results obtained for a dry polymer precursor showing thermal degradation.

of the organic material; a small amount of inert residue remains. As the temperature reaches (>540 °C), a complete burnout of organics can be achieved. This process occurs smoothly with an almost constant decomposition rate (calculated at 0.16%/°C) which reveals the great thermal stability of the polymer and suggests that the organic fiber shrinkage during calcination must occur radially to avoid breaking the wire.

3.2. FT-IR and XRD analyses

The Fourier transform-infrared (FT-IR) spectrum for the dry polymer used in the spin-stretching technique is illustrated in Fig. 3. Several bands are observed in the spectrum: OH band (3400 cm^{-1}), alkane C—H (2945 cm^{-1}), carbonyl stretching C=O (1728 cm^{-1}), ester O—C—O (1085 cm^{-1}) and bands in the regions of 1636, 1405 and 1244 cm^{-1} which are characteristics of

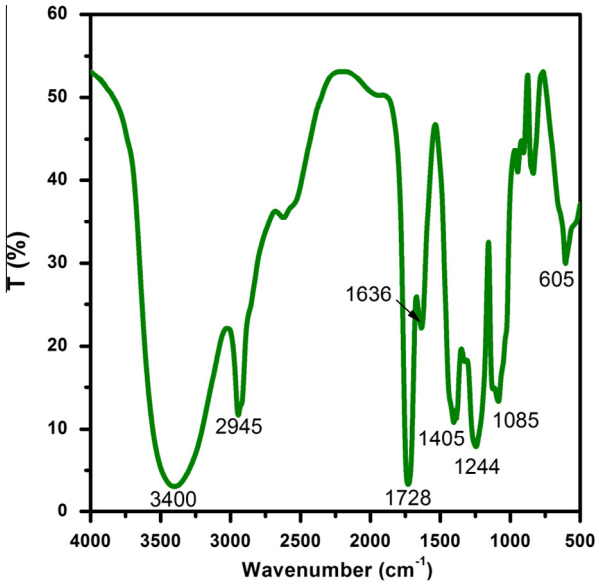

Fig. 3. FT-IR spectrum for the dry polymer (in KBr).

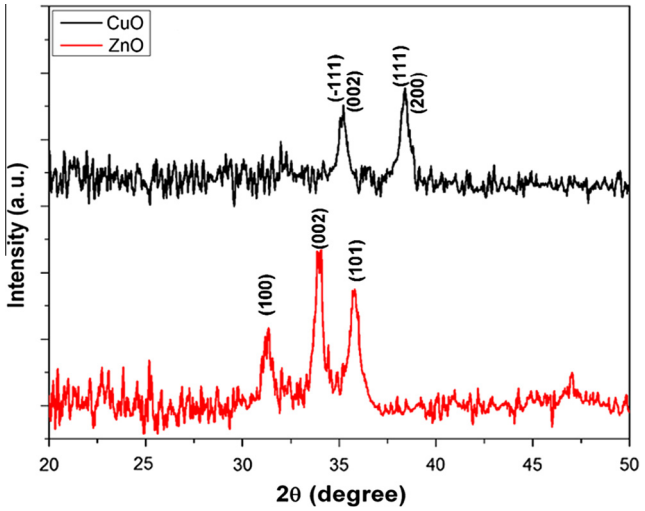

Fig. 4. XRD analysis of ZnO and CuO deposited nanofibers obtained by the spin-stretching technique after calcination at 550 °C for 2 h.

asymmetric and symmetric stretching of carboxyl groups and are responsible for the complexation of metallic cations. A long-chained polymer with residual carboxylic groups for complexation of the metallic cations was identified.

The XRD analysis of these nanofibers was performed to evaluate the crystallite size and crystalline phases (see Fig. 4). All peaks can be indexed to the monoclinic phase of CuO (JCPDS 89-2530); no impurity peaks are detected which indicates that CuO nanostructures are pure and crystalline. The CuO crystallite size estimated by the Scherrer equation was 15.9 ± 0.2 nm. The ZnO structure can be simply described as a non-central symmetric structure indexed as a hexagonal ZnO phase (JCPDS 79-208) with a crystallite size of 12.0 ± 0.7 nm. Peak intensities relative to the background signal demonstrates monoclinic and hexagonal phases of the products and the high crystallinity of the main phase. Characteristic peaks of $Zn(OH)_2$ and $Cu(OH)_2$ were not observed which indicates single phases. Nanocrystallites are oriented along [0 0 1] and [1 1 1] directions.

3.3. Morphological characterization of ZnO nanofibers

Many techniques have been exploited to generate thin fibers from a broad range of polymers, but the spatial orientation of such fibers is difficult to control. The spin-stretching technique can overcome these problems with a larger spatial control on the fiber orientation. The uniaxial alignment of nanowires on interdigital electrodes permits less material to be deposited with maximum electrical contacts which enhances the surface area of the oxide for better sensitivity in gas sensors, for example.

SEM images (see Fig. 5) confirm that ZnO ceramic nanofibers are uniformly deposited on the substrate. After calcination of organic fibers at 550 °C for 2 h, the formation of ZnO nanowires with good mechanical stability is evident. The uniaxial alignment can be achieved layer by layer to generate a 3D grid structure by just rotating the substrate by 90°. The SEM grid image corresponds to a small area of the substrate (120 μm^2), but homogeneity is observed in the whole substrate area (*ca.* 1 cm^2). This deposition area may be larger and will depend on dimensional configurations of cylinders used in the apparatus depicted in Fig. 1 and the stretchability of the polymeric composite. The morphology is composed of uniform ZnO nanofibers composed of nanoparticles of an approximate size (*ca.* 10 nm or less). In addition to the nanoparticulate aspect, ZnO wires exhibit a nanoporous characteristic which can increase the gas sensing performance due to a higher surface area. One undesired aspect of the technique is the heterogeneity in the diameter of the obtained ceramic fibers which are between *ca.* 50 and 500 nm. Better control of process variables can produce ceramic nanofibers of less than 100 nm because in practice the

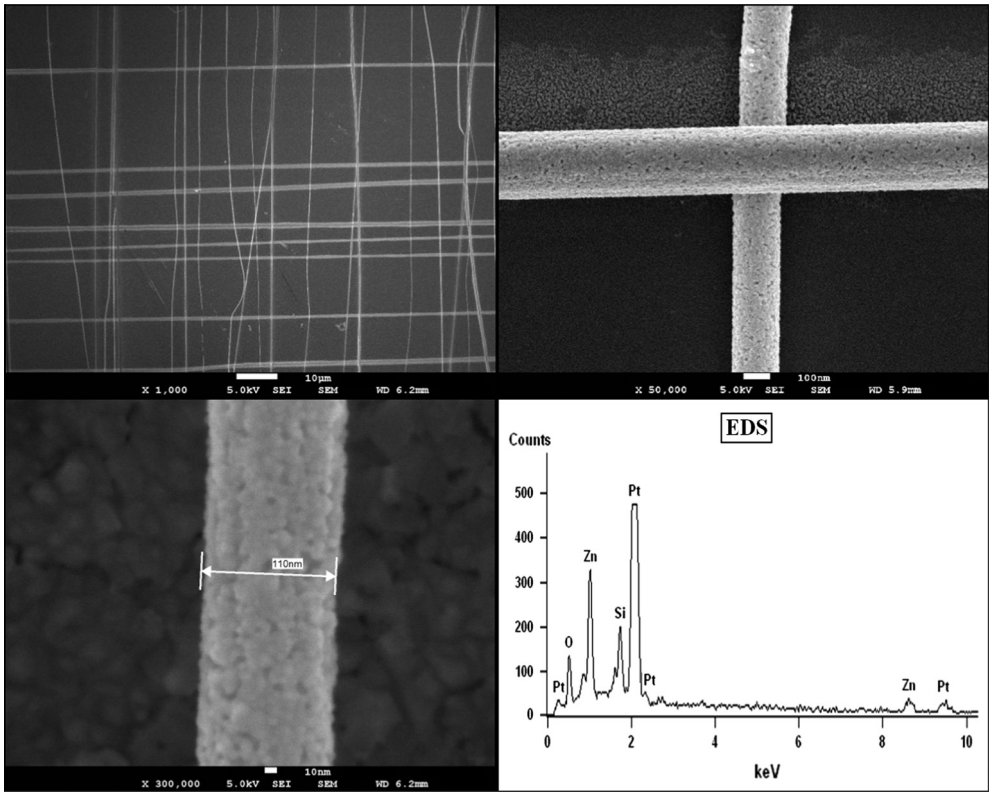

Fig. 5. ZnO nanofibers obtained by the spin-stretching technique after calcination at 550 °C for 2 h.

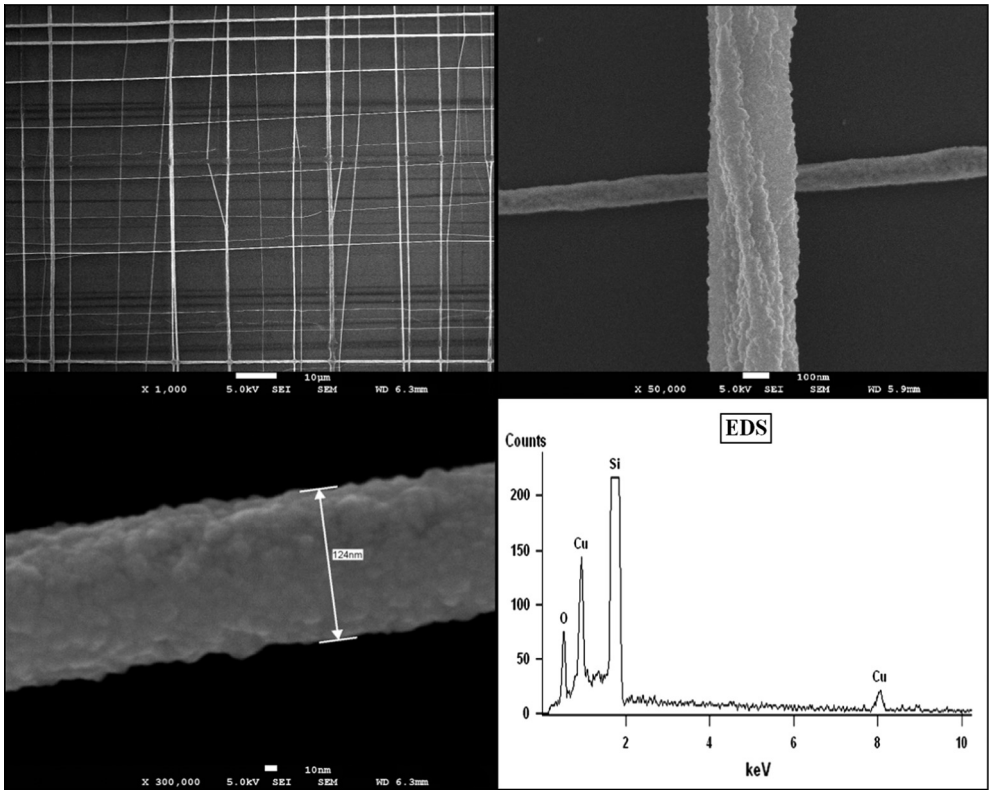

Fig. 6. CuO nanofibers obtained by the spin-stretching technique after calcination at 550 °C for 2 h.

higher the rotational speed of the cylinder (see Fig. 1), the thinner the organic fibers generated. Therefore, the apparatus is currently under development to produce better results.

The same trend can be noted for CuO nanofibers obtained by the spin-stretching technique (see Fig. 6) which attests that the method seems to be very reproducible with strong possibilities of obtaining different metal oxide nanofibers. The uniaxial alignment of ceramic nanofibers in a one-dimensional structure can add anisotropic features to the system which exhibit different electrical behavior (e.g., conductivity) as compared to three-dimensional films.

In our process, the starting point of nanofiber growth originates from crystal defects which are caused by the oriented attachment and by the coalescence process which is analogous to oriented attachment where two or more small crystallites can merge and then rotate to form a crystal. In this study, nanofibers were formed by the coalescence of fully elongated ZnO and CuO colonies which can occur only at the ends of each elongated unit. Similar behavior was observed in Al_2O_3 nanofibers fabricated by the electrospinning technique [35]. To better understand the growth process when nanocrystals grow via the oriented attachment, the high resolution-transmission electron microscopy (HR-TEM) technique should be employed. Finally, new experiments are under development to perform electrical conductivity and sensor characterizations of these nanofibers as well as experiments to apply this method for large-scale production and the potential application as a gas sensor.

4. Conclusions

A simple and versatile method was demonstrated to generate organic fibers uniaxially aligned (a spin-stretching technique). Calcination of these fibers containing metallic precursors of zinc and copper resulted in good ceramic nanofibers with an average diameter of 120 nm as well as hexagonal and monoclinic structures, respectively. The production of fibers with high deposition rates at low cost can be obtained by adjusting process variables. Potential applications of these ceramic nanofibers can be extended to various functional materials with electrical, magnetic and mechanical properties. This method would be attractive for large scale production.

Acknowledgments

The financial support of this research project by the Brazilian research funding agencies CNPq and FAPESP is gratefully acknowledged.

References

[1] N. Horzum, D. Tascioglu, S. Okur, M.M. Demir, Talanta 85 (2011) 1105–1111.
[2] T.-J. Hsueh, C.-L. Hsu, S.-J. Chang, I.C. Chen, Sens. Actuators, B – Chem. 126 (2007) 473–477.
[3] P.-S. Cho, K.-W. Kim, J.-H. Lee, J. Electroceram. 17 (2006) 975–978.
[4] S.-W. Choi, J.Y. Park, S.S. Kim, Chem. Eng. J. 172 (2012) 550–556.
[5] Y.-S. Kim, I.-S. Hwang, S.-J. Kim, C.-Y. Lee, J.-H. Lee, Sens. Actuators, B – Chem. 135 (2008) 298–303.
[6] L. Liao, Z. Zhang, B. Yan, Z.X. Shen, J.X. Zhang, T. Yu, Nanotechnology 20 (2009) 085203–085208.
[7] F. Dabirian, S.A.H. Ravandi, A.R. Pishevar, R.A. Abuzade, J. Electrostat. 9 (2011) 540–546.
[8] D. Li, Y.L. Wang, Y.N. Xia, Nano Lett. 3 (2003) 1167–1171.
[9] D.L. Carillo, Chem. Eng. Prog. 99 (2003) 43S–45S.
[10] J.T. Devreese, Importance of nanosensors: Feynman's vision and the birth of nanotechnology, Matt. Bull. 32 (2007) 718–724.
[11] J.C. Adamowski, N. Gilder, Sensores: Tecnologias e Aplicações, first ed., AlphaMidia Assessoria Fonografica, São Paulo, 2004.
[12] N. Barsan, U. Weimar, J. Phys.: Condens. Matter. 15 (2003) R813–R839.
[13] J.M. Madou, S.R. Morrison, Chemical Sensing with Solid State Devices, Academic Press Inc, San Diego, 1989.
[14] A.K. Prasad, P.I. Gouma, J. Mater. Sci. 38 (2003) 4347–4352.
[15] B.S. Archanjo, Sensores de gás e memoristores fabricados por oxidação anódica local utilizando microscopia de varredura por sonda, 118 f Universidade Federal de Minas Gerais, Belo Horizonte, Tese - Departamento de Física, 2009. 2009.
[16] D.H. Zhang, Z.Q. Liu, C. Li, T. Tang, X.L. Liu, S. Han, B. Lei, C.W. Zhou, Nano. Lett. 4 (2004) 1919–1924.

[17] F. Hernandez-Ramirez, A. Tarancon, O. Casals, J. Arbiol, A. Romano-Rodriguez, J.R. Morante, Sens. Actuators, B – Chem. 121 (2007) 3–17.
[18] C.N.R. Rao, F.L. Deepak, G. Gundiah, A. Govindaraj, Prog. Solid State Ch 31 (2003) 5–147.
[19] A. Kolmakov, M. Moskovits, Annu. Rev. Mater. Res. 34 (2004) 151–180.
[20] A.B. Gonçalves, Síntese de Nanofios de Óxido de Cobre (CuO) e Fabricação de Nanodispositivos, 85 f Dissertação – UNIVERSIDADE FEDERAL DE MINAS GERAIS, Belo Horizonte, 2008. 2008.
[21] Z. Charifi, H. Baaziz, Ali Hussain Reshak, Phys. Status Solidi B 244 (2007) 3154–3167.
[22] M. Bouderbala, S. Hamzaoui, B. Amrani, Ali H. Reshak, M. Adnane, T. Sahraoui, M. Zerdali, Physica B 403 (2008) 3326–3330.
[23] A.H. Reshak, J. Ebothe, A. Wojciechowski, W. Kuznik, A. Popeda, Physica E 42 (2010) 1769–1771.
[24] K. Ozga, T. Kawaharamura, A.A. Umar, M. Oyama, K. Nouneh, A. Slezak, S. Fujita, M. Piasecki, A.H. Reshak, I.V. Kityk, Nanotechnology 19 (2008) 185709–185714.
[25] J.T. Chena, F. Zhanga, J. Wanga, G.A. Zhanga, B.B. Miaoa, X.Y. Fana, D. Yana, P.X. Yana, J. Alloys Comp. 454 (2008) 268–273.
[26] Y. Du, R.Z. Chen, J.F. Yao, H.T. Wang, J. Alloys Comp. 551 (2013) 125–130.
[27] Y.X. Liu, E.Q. Xie, J. Alloys Comp. 506 (2010) 772–776.
[28] M. Zhao, X. Wang, L. Ning, X. Li, J. Alloys Comp. 507 (2010) 97–100.
[29] A. Ziabicki, Fundamentals of Fiber Formation, John Wiley and Sons, London, 1976.
[30] D. Li, Y.N. Xia, Adv. Mater. 16 (2004) 1151–1170.
[31] J. Doshi, D.H. Reneker, J. Electrostat. 35 (1995) 151–160.
[32] R. Parra, R. Savu, L.A. Ramajo, M.A. Ponce, J.A. Varela, M.S. Castro, P.R. Bueno, E. Joanni, J. Solid State Chem. 183 (2010) 1209–1214.
[33] L. Satyanarayana, K.M. Reddy, S.V. Manorama, Mat. Chem. Phys. 82 (2003) 21–26.
[34] H. Zheng, O.T. Sorensen, J. Eur. Ceram. Soc. 19 (1999) 1987–1996.
[35] P.-C. Yu, R.-J. Yang, Y.-Y. Tsai, W. Sigmund, F.-S. Yen, J. Eur. Ceram. Soc. 31 (2011) 723–731.